

# Dry Pre-Lithiation for Graphite-Silicon Diffusion-Dependent Electrode for All-Solid-State Battery

Jongjun Lee, Dahee Jin, Ju Young Kim,\* Youngjoon Roh, Hyobin Lee, Seok Hun Kang, Jaecheol Choi, Taejin Jo, Young-Gi Lee, and Yong Min Lee\*

The graphite/silicon-based diffusion-dependent electrodes (DDEs) are one of the promising electrode designs to realize high energy density for all-solid-state batteries (ASSBs) beyond conventional composite electrode design. However, the graphite/silicon-based electrode also suffers from large initial irreversible capacity loss and capacity fade caused by significant volume change during cycling, which offsets the advantages of the DDEs in full-cell configuration. Herein, a new concept is presented for DDEs, dry pre-lithiated DDEs (PL-DDEs) by introducing Li metal powder. Since Li metal powder provides Li ions to graphite and silicon even in a dry state, the lithiation states of active materials is increased. Moreover, the residual Li within PL-DDE further serves as an activator and a reservoir for promoting the lithiation reaction of the active materials and compensating for the active Li loss upon cycling, respectively. Based on these merits, ASSBs with PL-DDE exhibit excellent cycling performance with higher columbic efficiency (85.2% retention with 99.6% CE at the 200th cycle) compared to bare DDE. Therefore, this dry lithiation process must be a simple but effective design concept for DDEs for high-energy-density ASSBs.

## 1. Introduction

All-solid-state batteries (ASSBs) are considered an effective solution to overcome the prevailing problems associated with Li-ion batteries (LiBs), such as compromised safety and limited cell energy density.<sup>[1]</sup> The unique features of ASSBs, which consist of only solid components, can inherently solve the safety issues caused by flammable liquid electrolytes. Even with regard to energy density, ASSBs are expected to deliver sufficient energy and high power for long-range EV applications, taking compactly stacked bipolar cell configurations within battery packs.<sup>[2]</sup> However, to realize ASSBs with comparable or superior performance to conventional LiBs, multiple critical challenges must be addressed, such as enhancing the ionic/electronic conductivity and electrochemical stability window of solid electrolytes, optimizing the electrode design, and reducing the interfacial resistance.<sup>[3]</sup>

In particular, the electrode design principle should be more carefully devised for the development of ASSBs because fragile solid-solid contact between the active materials and solid electrolytes cannot guarantee sufficient electrochemical reactions and Li-ion transport at each interface.<sup>[4]</sup> A typical electrode design for ASSBs adopts composite electrodes with a uniform mixture of active materials and solid electrolyte particles, where Li-ion migration within this electrode is enabled via the solid electrolyte domain.<sup>[5]</sup> In this regard, the progress in composite electrode development is designed to further improve the Li-ion percolation pathway by considering the spatial arrangement of the active material and solid electrolytes, such as shape modification and relative dimension ratio control of the active material and solid electrolyte particles.<sup>[6]</sup> However, composite electrodes still suffer from many practical challenges, including limited cell energy density and complex electrode fabrication.<sup>[7]</sup>


In contrast to composite electrodes, our group has successfully demonstrated diffusion-dependent electrodes (DDEs) that can deliver a high energy density with a simple fabrication process.<sup>[8]</sup> DDEs, which consist of only active materials and a small amount of polymeric binder without any solid electrolytes, transfer Li ions by interparticle ionic diffusion among the active materials. The absence of solid electrolytes within the

J. Lee, D. Jin, Y. Roh, H. Lee, Y. M. Lee  
Department of Energy Science and Engineering  
Daegu Gyeongbuk Institute of Science and Technology (DGIST)  
Daegu 42988, Republic of Korea  
E-mail: yongmin.lee@dgist.ac.kr

J. Y. Kim, S. H. Kang, J. Choi, Y.-G. Lee  
Materials and Components Research Division  
Electronics and Telecommunications Research Institute (ETRI)  
218 Gajeongno, Yuseong-gu, Daejeon 34129, Republic of Korea  
E-mail: juyoung@etri.re.kr

T. Jo  
Iljin Materials  
Seoul 04167, Republic of Korea

Y. M. Lee  
Energy Science and Engineering Research Center  
Daegu Gyeongbuk Institute of Science and Technology (DGIST)  
Daegu 42988, Republic of Korea

 The ORCID identification number(s) for the author(s) of this article can be found under <https://doi.org/10.1002/aenm.202300172>

© 2023 The Authors. Advanced Energy Materials published by Wiley-VCH GmbH. This is an open access article under the terms of the Creative Commons Attribution-NonCommercial License, which permits use, distribution and reproduction in any medium, provided the original work is properly cited and is not used for commercial purposes.

DOI: 10.1002/aenm.202300172

electrode provides significant advantages in terms of volumetric and gravimetric energy densities. Furthermore, the critical fabrication issues of the composite electrode, such as ensuring the chemical stability of the solid electrolytes and the formation of a well-connected solid electrolyte pathway within the composite electrode, are not needed to be considered in the DDEs.<sup>[9]</sup> These outstanding merits of DDEs have attracted considerable interest as promising electrodes for high-performance ASSBs. For facile interparticle ionic diffusion, the mechanical properties of active materials in a delithiated/lithiated state are essential, and our previous works validated that the DDE structure successfully realized high-performance ASSBs with graphite, titanium disulfide, and graphite/silicon (Gr/Si) electrodes with high mass loading.<sup>[8]</sup> In particular, a recent study demonstrated that intra- and inter-diffusion of graphite and silicon particles can achieve highly compact electrodes and high energy density ( $\sim 997 \text{ mAh cm}^{-3}$ ), along with good rate capability.<sup>[8]</sup> However, although the Gr/Si electrode is a promising candidate to improve the cell energy density, the inherent issue of high volumetric expansion of silicon upon lithiation ( $\sim 400\%$ ) leads to Li source loss, silicon particle cracking, electrode expansion, and constant breakage/reformation of solid electrolyte interphase (SEI), which results in lower initial Coulombic efficiency (CE) and severe capacity fading.<sup>[10]</sup>

To address the aforementioned issues, pre-lithiation can be an effective strategy for alleviating the problems with silicon.<sup>[11]</sup> The pre-lithiated Li ions in the electrode not only improve the low first CE of the Gr/Si electrode by compensating for the irreversible capacity loss in the first charge/discharge cycle but also decrease the average potential of the negative electrode and consequently increase the cell average potential.<sup>[11,12]</sup> Furthermore, it can mitigate volume expansion issues, such as silicon particle cracking and electrode structure degradation, because the pre-volume change can alleviate the extreme volume

expansion/contraction of silicon during cycling.<sup>[11,13]</sup> Currently, there are four main pre-lithiation methods for anode materials: chemical pre-lithiation,<sup>[14]</sup> electrochemical pre-lithiation,<sup>[15]</sup> pre-lithiation using lithiated active materials,<sup>[16]</sup> and pre-lithiation by direct contact with lithium metal.<sup>[12,17]</sup> However, some of these methods are difficult to apply to ASSB because of the complex manufacturing process of the composite electrode and the high reactivity of the solid electrolyte. Hence, a few papers have reported the effect of pre-lithiation on electrodes for ASSB.<sup>[18]</sup> However, because DDEs have a simple structure and are easy to fabricate, the introduction of the pre-lithiation method into DDEs is easily possible.<sup>[8]</sup>

Herein, we propose a new pre-lithiation method for DDEs in the dry state via direct contact with Li metal powder. In contrast to conventional pre-lithiation strategies that use additional solvents, gases, and additives, this strategy induces a pre-lithiation reaction in the dry state, which can be a straightforward process and prevents undesired side reactions. With the simultaneous addition of Li metal powder to the electrode, we found that the initial CEs were improved by compensating for Li loss even in the solid state. Moreover, the added Li metal particles serve as an extra reservoir to counterbalance the active Li loss because of anode deterioration during cycling. The lithiation behavior of the ASSBs was systematically investigated using electrochemical measurements, X-ray diffraction (XRD), and scanning electron microscopy (SEM). Furthermore, we verified that pre-lithiated DDE (PL-DDE) consistently exhibited better electrochemical performance in LCO||Gr/Si DDE full cells.

## 2. Results and Discussion

**Figure 1** illustrates the fabrication process of a dry pre-lithiated (PL) DDE electrode using Li metal powder. The fabrication

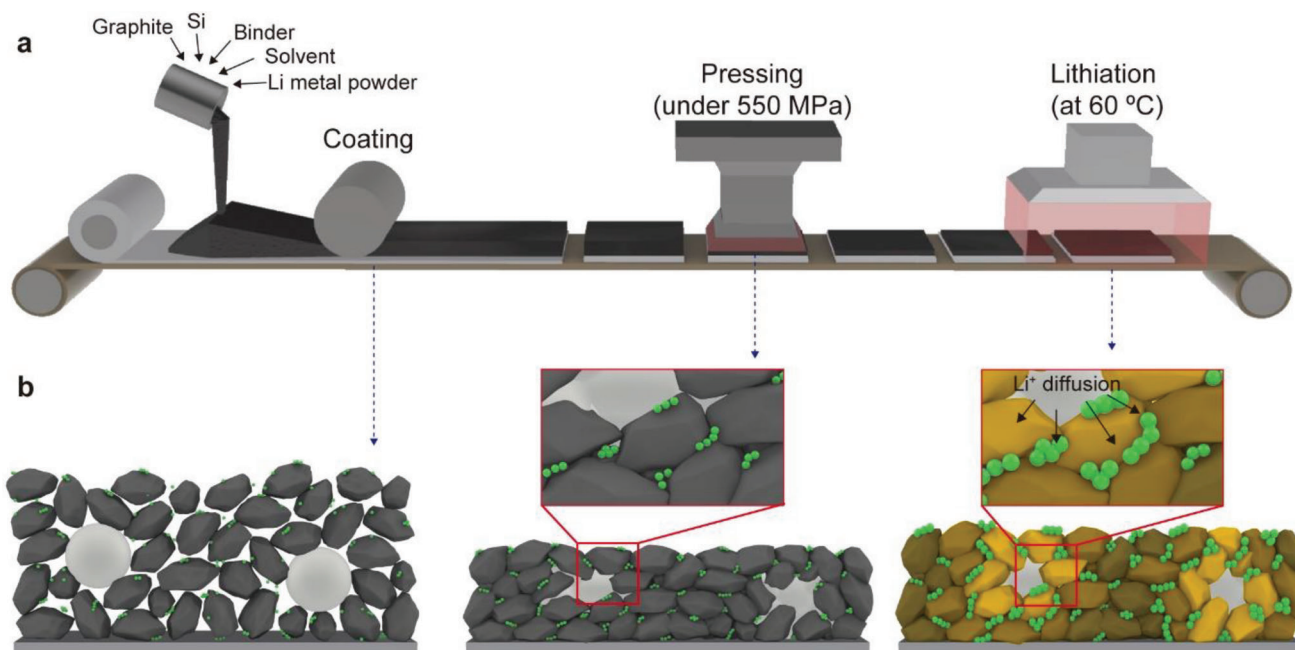


**Figure 1.** Schematic illustrations of a) the PL-DDE fabrication process, including the slurry coating, pressing, and dry pre-lithiation process, and b) the structural and lithiation state changes in each fabrication step.

process involved the conventional slurry-mixing of Gr/Si active materials, a polymeric binder, an organic solvent, and Li metal powder, followed by coating and lithiation of Li at 550 MPa and 60 °C. At this time, 1, 3, and 5 wt% of Li metal powder were added relative to the active material, and each electrode was denoted as PL-DDE 01, 03, and 05, respectively. This pressure-induced lithiation is a crucial step in cracking the  $\text{Li}_2\text{CO}_3$  protection layer on the surface of Li metal powder and it enables direct contact between the Li metal and active materials.<sup>[19]</sup> In contrast to other pre-lithiation strategies, such as chemical or electrochemical pre-lithiation and the use of lithiated active materials, our method is simple and readily applicable to commercial LiB electrode fabrication processes. Moreover, the lithiation process can be performed in a dry state without any solvents, gas, additives, or additional processes that can cause side reactions among electrode components. In addition, it could improve the uniformity of lithiation and prevent electrode deterioration caused by the different lithiation states, because the Li metal powder was evenly dispersed in the electrode (Figure 1b). In particular, DDEs utilize interparticle ionic diffusion, and thus, Li-ion movement among the active material particles can continue until the Li-ion gradient in the electrode is completely relieved. Therefore, uniform pre-lithiation can be realized using this method. In this regard, the formation of conformal contact between the solid components is important under sufficient pressure. The optical images of the PL-DDEs exhibit the considerable effect of the applied pressure (Figure S1, Supporting Information). After activating Li in a dry state for 10 h, the DDE under high pressure showed that the shiny Li metal deposits had mostly disappeared, whereas Li metal powder was retained for DDEs applied under lower pressure. To further demonstrate the transport of the pre-lithiated Li ions throughout the whole electrode, the DDE, one side of which a Li metal plate was attached, was prepared as an extreme case of pre-lithiation, and the opposite side was observed by optical microscopy. Graphite experiences distinct discoloration depending on the lithiated state. Figure S2 and Movie S1, Supporting Information visualize the effective pre-lithiation process by the color change. These results indicate that Li ions that were transported from the Li metal plate at the opposite side can efficiently pre-lithiate the whole active material particles even in a dry state if enough Li source was provided, which means that overlithiation of active material particles near the Li metal powders can be prevented. Overall, pre-lithiation of DDE using Li metal powder is a potentially effective and simple method for improving the performance of Gr/Si electrodes. Nonetheless, the pre-lithiation of ASSBs under dry conditions remains challenging for practical applications. Several factors affect the pre-lithiation behavior when Li metal powder is used, including the amount of Li metal powder, pre-lithiation temperature, and time. Also, the change in the lithiation state is closely related to the electrochemical performance, which significantly influences the volume expansion behavior of the Si-based electrodes. Therefore, it is essential to optimize the pre-lithiation conditions to mitigate electrode degradation and enhance electrochemical performance.

First, we investigated the change in the lithiation behavior in the dry state depending on the amount of Li metal powder (Figure 2). As shown in Figure S3, Supporting Information, the Li metal powder is homogeneously distributed in the active materials after the electrode fabrication. After compressing the elec-

trode, the SEM image of the bare DDE shows dense morphologies in which the active material particles are packed closely enough to transport Li ions via interparticle ionic diffusion (Figure 2a). Regardless of the amount of Li, the morphologies of the PL-DDEs are slightly different from that of the bare electrode (Figure 2b–d). After pressing, the lithiation of graphite and silicon, namely Li-ion transport from the Li metal powder and neighboring active material particles, occurs immediately. Thus, vacancies are observed at the initial locations of the Li metal powders. In addition, the bright area is radially exhibited based on the vacancy, which may imply lithiated active materials through interparticle ionic diffusion. The aforementioned brighter region and vacancies on the surface became more visible as the amount of Li metal powder increased. After completing Li pre-lithiation, the PL-DDE samples showed slightly different morphologies compared to SEM images after pressing. For PL-DDE 01 (Figure 2f), lithiated graphite and silicon can be distinguished by the contrast due to the low lithiation state of the active materials. In contrast, SEM images with low contrast difference were observed for the DDEs with higher Li metal powder (Figure 2g,h). The magnified SEM images after the pre-lithiation process further illustrated the detailed structural change for each PL electrode (Figure 2i–l). In PL-DDE 03 and PL-DDE 05, the entire electrode surface was covered by lithiated silicon particles appearing in light gray (Figure 2k,l). It is worth noting that the uniform brightness indicates uniform lithiation of the entire electrode without local overlithiation of several active material particles located near the Li metal powders even in a dry state. In addition, the vacancies are almost filled with lithiated active materials, especially silicon, owing to the high-volume expansion compared to that of graphite (Figure 2f–h). The cross-sectional SEM images also suggest that the thickness of PL-DDEs slightly increases by ~10% due to lithiation into active materials (Figure S4, Supporting Information). These morphological changes indicate the phase transformation of crystalline silicon (c-Si) to amorphous lithiated silicon (a- $\text{Li}_x\text{Si}$ ) or  $\text{c-Li}_{15}\text{Si}_4$  upon silicon lithiation.<sup>[20]</sup> However, PL-DDE 05 still shows pores on the surface, which may hinder Li-ion diffusion in the subsequent electrochemical reaction (Figure 2h). Conversely, the morphological change of graphite during lithiation was difficult to observe by SEM because graphite shows a relatively low volume change, and lithiated silicon particles covered most of the electrode surface (Figure 2g,h), except for DDE with low Li content (Figure 2f).

To further reveal the lithiation state of graphite and silicon, XRD was performed before and after the pre-lithiation process in the dry state (Figure 2m,n). All the DDEs show the characteristic reflections of graphite (002) at  $2\theta \sim 26.8^\circ$  and of the ordered (111) planes of c-Si at  $2\theta \sim 28.6^\circ$  before compression (Figure 2m).<sup>[21]</sup> After Li pre-lithiation in the dry state, graphitic lithiation patterns are detected in PL-DDE, corresponding to  $2\theta \sim 25.8^\circ$  ( $\text{LiC}_{18}$ ) and  $2\theta \sim 24.1^\circ$  ( $\text{LiC}_6$ ) (Figure 2j).<sup>[20,22]</sup> This indicates that the lithiation is initiated from graphite adjacent to Li metal powder and Li ions on the lithiated graphite are diffused to other graphite particles. However, the  $\text{c-Li}_{15}\text{Si}_4$  peak associated with fully lithiated silicon is elusive for all PL-DDEs after the pre-lithiation process. Unfortunately, it is difficult to achieve deeper lithiation of silicon by only contacting Li under dry conditions, probably because of the relatively slow Li diffusion rate and the low electronic conductivity of silicon.<sup>[8d]</sup> However,

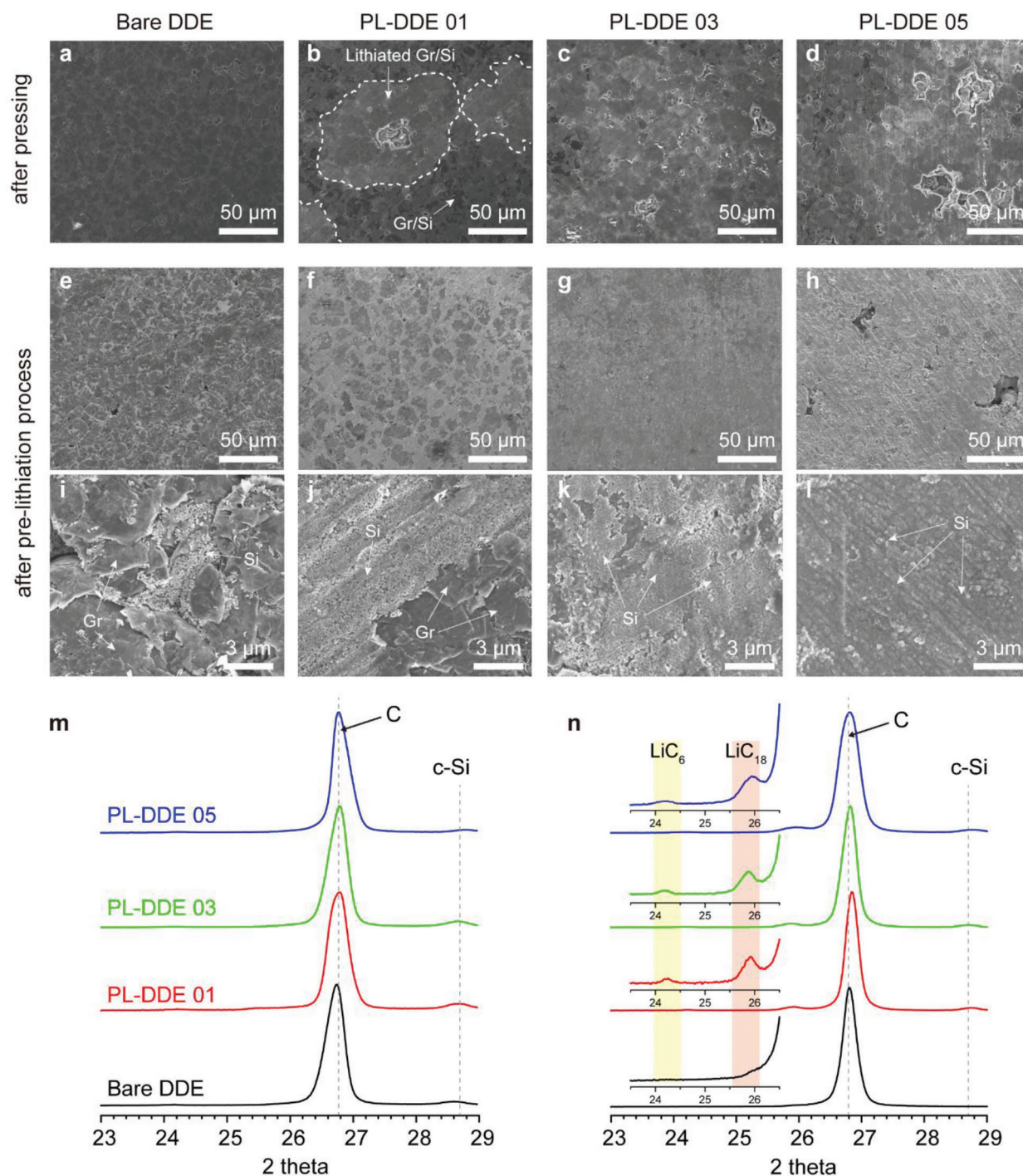


**Figure 2.** SEM images of each DDE after a–d) pressing and e–l) pre-lithiation process. XRD patterns of DDEs with different amounts of Li metal powder m) before and n) after pre-lithiation.

amorphous lithiated silicon with a low lithiation state can be induced by close contact with Li and lithiated graphite.<sup>[12,20]</sup> This amorphous lithiated silicon cannot be observed by XRD,<sup>[23]</sup> but the SEM images displayed in Figure 2 provide evidence of a volume expansion in the lithiation state of silicon from crystalline silicon to amorphous lithiated silicon. In addition, the optical image shows that the PL-DDE has residual Li that is not engaged in

the lithiation reaction, which is expected to react with active materials to provide the Li sources during cycling (Figure S5, Supporting Information). The reason why all the Li metal powders do not participate in the pre-lithiation process might be due to the loss of contact between the Li metal powder and active material. For this dry pre-lithiation process, the close contact between the Li metal and active materials is highly important for Li ions

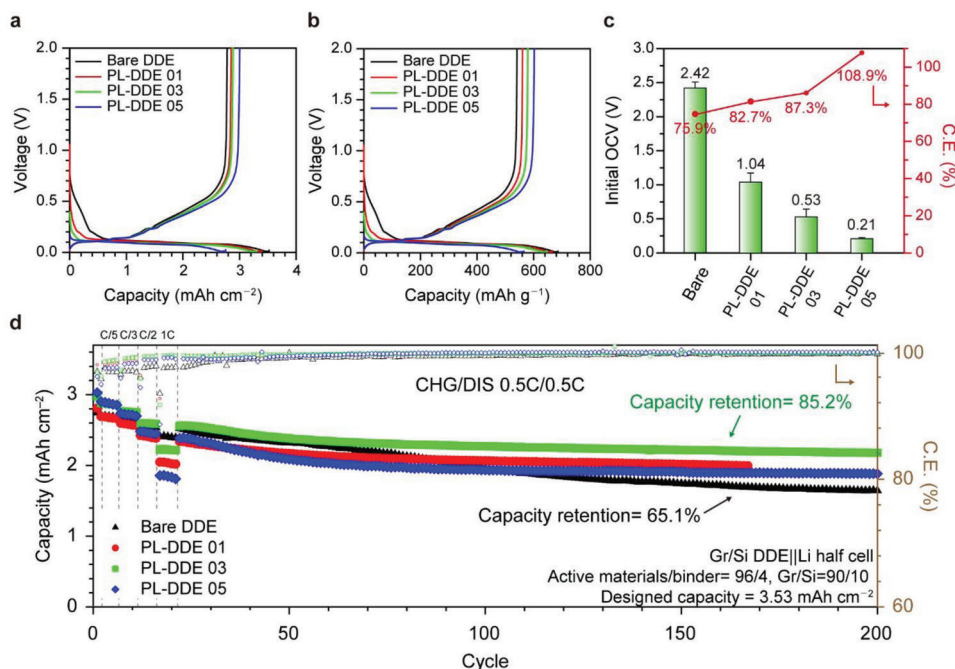


**Figure 3.** First charge-discharge voltage profiles of the Gr/Si||Li half-cells with DDEs versus a) areal capacity and b) specific capacity. c) Initial open circuit voltage (OCV) and CEs of Gr/Si||Li half-cells with DDEs. d) Rate capability and cycle performance of the Gr/Si||Li half-cells with DDEs.

to transport from Li metal to active materials. However, the vacancies can be generated at the interface between the Li metal and active materials owing to the competitive Li kinetics at each position (Figure S6, Supporting Information). The Li-ion transport is generally faster than the self-diffusion of Li in the Li metal powder.<sup>[24]</sup> Thus, all void made by the Li-ion transport into active materials is not filled with self-diffused Li from the core of the Li metal powder. Also, the 3D large reaction area may further accelerate vacancy generation. As a result, continuous vacancy injection into the Li metal could lead the Li metal powder to separate from the surrounding active material, resulting in residual Li. To further investigate the lithiation state of active materials in DDEs after the pre-lithiation process, XPS analysis was conducted on the bare DDE and PL-DDE 03 before and after pre-lithiation (Figure S7, Supporting Information). For the bare DDE, no significant difference in both C 1s and Si 2p spectra was observed after the pre-lithiation process. In contrast, for the PL-DDE 03, a small  $\text{Li}_x\text{C}$  peak was detected at around 283 eV,<sup>[25]</sup> indicating the successful lithiation of a certain amount of graphite. In addition, the Si 2p spectra of PL-DDE 03 also showed notable changes after pre-lithiation. The  $\text{Li}_x\text{Si}$  and  $\text{Li}_x\text{SiO}_y$  peaks were observed at around 97 and 101 eV, respectively.<sup>[26]</sup> These peaks represent the lithiation of Si and  $\text{SiO}_x$ , which indicates that dry pre-lithiation with Li metal powder can successfully lithiate the active materials in DDE.

To figure out the effects of pre-lithiation and residual Li on electrochemical performance, the Gr/Si||Li half-cells were tested at 60 °C (Figure 3). The electrochemical impedance spectroscopy after assembling the cell showed a gradual decrease in the interface ( $R_{\text{inter}}$ ) and charge transfer resistance ( $R_{\text{ct}}$ ) as the amount of Li metal powder increased (Figure S8, Supporting Information). This is most likely attributed to the decomposition products of

LPSCl at the interface between the Li metal powder and LPSCl solid electrolyte layer.<sup>[27]</sup> LPSCl has low chemical stability with Li metal powder, and thus the LPSCl, which is in contact with Li metal, can be decomposed to the stable but resistive components. As the amount of Li metal powder in the electrode increases, the resistive area increases and accordingly, the measured resistance can decrease. Figure S8, Supporting Information also displays the Li-ion diffusion term regardless of Li metal contents in the low-frequency range, which suggests successful lithiation even in a dry state. The cycling voltammetry was performed for the bare DDE and PL-DDEs (Figure S9, Supporting Information). Consistent peaks corresponding to the electrochemical reaction of graphite and silicon were observed, which indicates that direct Li metal deposition in the electrode was minimized. After fabricating the Gr/Si||Li half-cells, the cells were allowed to rest for 2 h before electrochemical testing to stabilize the cell. After cell assembly, a higher amount of Li metal powder led to an overall lower open-circuit voltage (OCV), which indicated a higher degree of active material lithiation and contribution of the Li metal powder at the interface between the PL-DDEs and solid electrolyte layer (Figure S10, Supporting Information). Then, OCV was stabilized to slightly higher values after resting for 2 h, which means that Li ions further undergo a lithiation reaction into entire active materials via interparticle diffusion of Li ions (Figure S10, Supporting Information).

Figure 3a,b shows the voltage profiles of the Gr/Si||Li half-cell in the first cycle. In the potential profile of bare DDE, the voltage plateau appeared at 0.3–0.8 V during the first charge, which represented the irreversible capacity loss caused by the decomposition of the solid electrolyte. With an increase in the lithiation state of PL-DDEs, the voltage plateau is remarkably reduced, implying that pre-lithiated active materials and residual Li can

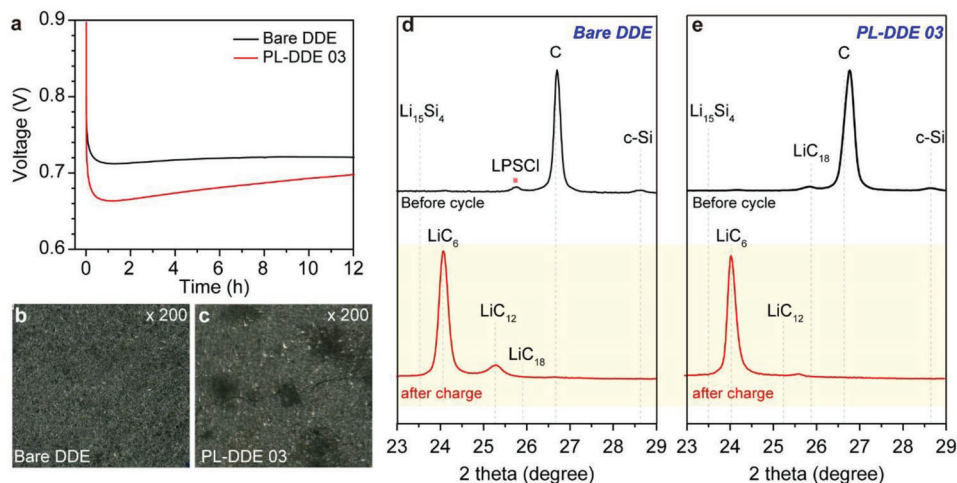


**Figure 4.** a) The OCV profiles during a 12 h rest period after the first cycle and b,c) optical images of the bare DDE and PL-DDE 03 after the initial charge-discharge cycle. XRD patterns of d) the bare DDEs and e) PL-DDE 03 before and after lithiation.

compensate for active lithium loss. Meanwhile, the first discharge capacity of PL-DDEs only reaches  $\sim 3.38$ , 3.30, and 2.76 mAh cm<sup>-2</sup>, respectively, significantly less than the 3.52 mAh cm<sup>-2</sup> in the bare DDE, confirming the partial lithiation behavior. Benefiting from pre-lithiation, the first charge capacity of PL-DDEs reached 2.85, 2.88, and 3.0 mAh cm<sup>-2</sup>, respectively, while bare DDE (2.78 mAh cm<sup>-2</sup>) suffered from huge capacity loss. In particular, PL-DDE 05 showed a comparable capacity of 602.1 mAh g<sup>-1</sup> with the theoretical capacity of the Gr/Si electrode ( $\sim 621$  mAh g<sup>-1</sup>), suggesting that the pre-lithiation strategies can realize the high energy density of ASSBs. Figure 3c summarizes the initial potential profiles of all the DDEs, including the initial OCVs and CEs. The CEs of the Gr/Si||Li half-cells tend to increase as the OCV decreases. Moreover, the cell with PL-DDE 05 exhibits a CE of  $\sim 108.9\%$ , which far exceeds that of the bare cell (75.9%). The stable charge/discharge behavior of PL-DDE in the first cycle constantly improves the CEs in subsequent cycles, compared to the bare DDE, which implies that the residual Li could support the enhancement of reversible active Li utilization (Figure S11, Supporting Information).

While the PL-DDEs delivered a higher capacity at 0.1 C, their capacities decrease relatively at C-rates higher than 0.5 C because of the vacancies in the electrode (Figure 3d). The vacancies in the electrode hinder the diffusion of Li ions between the active materials within the PL-DDEs, which leads to an increase in the tortuosity of the diffusion pathways. Although the vacancies created at the location of Li metal powder were almost filled with volume expansion of lithiated active materials as observed in Figure 2, the 16.6 vol% of additional vacancies can be generated within the PL-DDE 05 than the bare DDE, given that all of the Li was extracted in the delithiation reaction (Figure S12 and Table S1, Supporting Information). Another possible reason is that Li<sub>2</sub>CO<sub>3</sub> resistive materials coated on the Li metal powder remain after compression, impeding the electronic and ionic flux within the electrode. To investigate the effects of the abovementioned vacancies and Li<sub>2</sub>CO<sub>3</sub> residues on the rate performance of DDEs, the diffusion coefficients of the bare DDE and PL-DDE 03 were investigated using the galvanostatic intermittent titration technique (GITT) (Fig-

ure S13, Supporting Information). PL-DDE 03 exhibits a slightly lower average chemical diffusion coefficient of  $0.87 \times 10^{-9}$  cm<sup>2</sup> s<sup>-1</sup> compared to that of the bare DDE ( $1.43 \times 10^{-9}$  cm<sup>2</sup> s<sup>-1</sup>), which can lead to the lower rate performance of PL-DDEs. Nonetheless, the cell with only 1 wt% Li in the DDE (PL-DDE 01) shows significantly enhanced cycling performance (capacity retention of 85.2% after 150 cycles) compared to the cell with the bare DDE (capacity retention of 66.7% after 150 cycles) (Figure 3d). The cycling stability was further improved by increasing the lithiation state (PL-DDE 03, capacity retention of 86.0% after 150 cycles), and PL-DDE 05 also showed reasonable capacity retention of 79.5% after 150 cycles. The enhanced capacity retention of PL-DDEs than the bare DDE is most likely attributed to the vacancies induced by Li metal powders. Volume expansion/contraction during lithiation/delithiation might be alleviated by these vacancies, which contributes to the structural robustness of PL-DDEs. Based on these results, the optimum amount of Li metal powder for pre-lithiation was determined to be 3 wt%, and the following electrochemical results were obtained using this optimized composition. Another notable result of PL-DDE 03 is its initial CEs. The cell with bare DDE showed low CEs around 98.6% during 100 cycles, which indicates continuous active Li loss and severe capacity degradation (capacity retention of 65.1% after 200 cycles). In contrast, the cell with PL-DDE 03 achieved higher and stable CEs values of 99.4% even during the initial 100 cycles, resulting in capacity retention of 85.2% after 200 cycles.

To explain the dramatic improvement in PL-DDE 03, the change in the lithiation state after the first cycle was investigated by monitoring the OCV. The OCV curves were recorded over a long period after the first cycle to closely track the evolution of the OCV in the Gr/Si||Li half-cell (Figure 4a). After fully charging the cell, the OCV of the bare DDE immediately saturates to 0.72 V. In strong contrast, the OCV of PL-DDE 03 initially drops to 0.66 V and continuously increases to 0.70 V until 12 h, indicating that the residual Li within PL-DDE 03 is lithiated into the active materials, which is consistent with the results of Figure S10, Supporting Information.<sup>[13,28]</sup> The optical image in the PL-DDE 03 after the first cycle still shows a few shiny particles that look

like Li, which could participate in the subsequent lithiation reaction (Figure 4b,c). Unlike the previous pre-lithiation strategies, in which all lithium sources contribute to the first CE, Li metal powders still remain in PL-DDE because of the above-mentioned characteristics of the dry state lithiation process, which can serve as a further activator to promote additional lithiation of active materials during cycling. Moreover, the extra Li acts as a reservoir to counterbalance the active lithium loss owing to anode deterioration, thereby enhancing further cycling.

The role of residual Li within PL-DDE 03 was further demonstrated by XRD after full lithiation. In general, fully lithiated graphite and silicon undergo a phase change from C and c-Si to  $\text{LiC}_6$  and  $\text{Li}_{15}\text{Si}_4$ , showing a reflection shift in the lower  $2\theta$  region. However, some of the patterns associated with graphite lithiation in the bare DDE also exhibit a weak peak intensity of  $\text{LiC}_{12}$  ( $2\theta \sim 25.3$ ), implying that some of the graphite had a lower state of lithiation (Figure 4d).<sup>[20–22]</sup> In addition, there is no sign of the  $\text{Li}_{15}\text{Si}_4$  phase in the XRD pattern of the bare DDE. These results imply that diffusion-based Li-ion transport cannot utilize all active materials. In contrast, PL-DDE 03 exhibits fully lithiated graphite in the form of  $\text{LiC}_6$  (Figure 4e). This can be explained by the presence of Li within PL-DDE 03, which provides the Li source to the active materials and induces the uniform lithiation of the entire DDE during cycling. It is worth noting that uniformly and fully utilized DDEs can achieve higher specific capacities and CEs. This phenomenon persisted even after the 100 cycles (0.5/0.5 C charge/discharge). The PL-DDE 03 still only exhibited the  $\text{LiC}_6$ , while the bare DDE showed an increased  $\text{LiC}_{12}$  peak (Figure S14, Supporting Information). This result suggests that the residual Li helps efficient lithiation of the active material even during long-term cycling. Despite the help of Li sources, the fully lithiated  $\text{Li}_{15}\text{Si}_4$  phase was also difficult to find in PL-DDE 03, which means that there is still room for improvement with a more optimized pre-lithiation condition. For more detailed information, XPS analysis was also conducted on the bare DDE and PL-DDE after the pre-lithiation process, lithiation, and delithiation (Figures S15 and S16, Supporting Information). As mentioned earlier,  $\text{Li}_x\text{Si}$ ,  $\text{Li}_x\text{SiO}_y$  were formed in the pre-lithiation process (Figures S15a and S16a, Supporting Information). The  $\text{Li}_x\text{SiO}_y$  is well known to be (electro)chemical stable, which is one of the major contributors to the irreversible capacity of silicon. Especially, DDEs in this work use nanometer-scale silicon, and the abundance of the oxidized surface can significantly affect the initial CEs. Our dry pre-lithiation process can compensate for the capacity loss during lithiation/delithiation through the formation of  $\text{Li}_x\text{SiO}_y$  at the pre-lithiation step. Meanwhile, Figure S17, Supporting Information suggests that residual Li is observed in the XRD pattern during the charge/discharge step. The detailed XRD patterns of the bare DDE and PL-DDE 03 are presented in Figure S17, Supporting Information.

Because the lithiation state is closely related to the volume expansion of Si-based electrodes, we performed SEM analysis after the charge and discharge processes. As shown in Figure 5a,d, both electrodes have similar thicknesses in the pristine condition. After lithiation, the bare DDE shows huge anode swelling of  $\sim 88\%$  (49  $\mu\text{m}$ ) (Figure 5b). In contrast, PL-DDE 03 mitigated the volume expansion (40  $\mu\text{m}$ ), as shown in Figure 5e, which is attributed to the pre-volume increase during the pre-lithiation process. In addition, this can be explained that the residual Li metal

powder serves as an additional binding point for active materials owing to its ductile and sticky properties, which suppressed the expansion of the active materials. After delithiation, significant volume change was not observed for both DDEs (Figure 5c–f), but suppressing the volume expansion of PL-DDEs at the lithiated state prevents damage to the active materials, enhancing the cycle performance. To demonstrate this, the adhesion strength for the bare DDE and PL-DDE was evaluated by the surface and interfacial characterization analysis system (SAICAS), which is a useful tool to delicately measure adhesion strength at a desired position by controlling the cutting depth. The electrodes before pressing showed similar adhesion strength, but the dramatic change was confirmed after pressing (Figure S18, Supporting Information). While the adhesion strength of the bare DDE only increases by 44% ( $0.31 \text{ N m}^{-1}$ ), the adhesion strength of the PL-DDE 03 is significantly improved by 245% ( $0.64 \text{ N m}^{-1}$ ), which implies that the residual Li can contribute to mitigating the volume expansion by tightly binding the neighboring solid components. Furthermore, the cross-sectional SEM analysis was performed to confirm the aforementioned effect on PL-DDE 03 after 100 cycles (Figure S19, Supporting Information). After long-term cycling, the bare DDE exhibited severe electrode deterioration with tremendous anode swelling of 196% and 150% for lithiation and delithiation, respectively. In strong contrast, the PL-DDE 03 mitigated the electrode degradation associated with the volume expansion of the electrode compared to bare DDE even after long-term cycling. Based on these findings, we summarize the lithiation behavior of PL-DDEs compared to bare DDE during cycling (Figure 5g). Even in the dry state, pre-lithiation can be realized by forming a conformal contact between Li and the active materials under sufficient pressure. Pre-lithiation occurs continuously between Li and an adjacent active material through the interparticle diffusion of Li via a concentration gradient. However, some of the Li might lose diffusion pathways because of the vacancies created between Li and neighboring active materials during the pre-lithiation process, which leads to the formation of residual Li within the electrode. Residual Li could be reactivated by contact with active materials owing to its volume expansion during lithiation. At this moment, residual Li plays an important role in promoting the lithiation reaction of the active materials and compensating for the active lithium loss during cycling. Therefore, the PL-DDEs achieved a uniform lithiation state with high utilization of the active materials, improving cycle performance and CEs. In contrast to PL-DDE, the bare DDE suffers from an uneven lithiation state of active materials because it only uses interparticle diffusion during lithiation, and the excessive volume expansion of the bare DDE leads to the continuous capacity loss, which is difficult to be fully compensated without pre-lithiation.

Based on the above results, the electrochemical performance of  $\text{LiCoO}_2$  (LCO)||Gr/Si DDE full cells was investigated. To exclude side reaction issues at the cathode, LCO composite cathode was prepared using a  $\text{Li}_3\text{InCl}_6$  halide electrolyte with a stable electrochemical window and low reactivity for LCO. At the first charge/discharge cycle at 0.1 C, the cells with PL-DDE 03 showed an areal capacity of  $\sim 2.66 \text{ mAh cm}^{-2}$ , benefiting from the pre-lithiation effect, whereas the cell with bare DDE exhibited a relatively lower capacity of  $\sim 2.53 \text{ mAh cm}^{-2}$  (Figure 6a). Moreover, in terms of CE, the cell with PL-DDE exhibited a remarkably improved CE of 84.8% compared to bare DDE (73.3%), suggesting

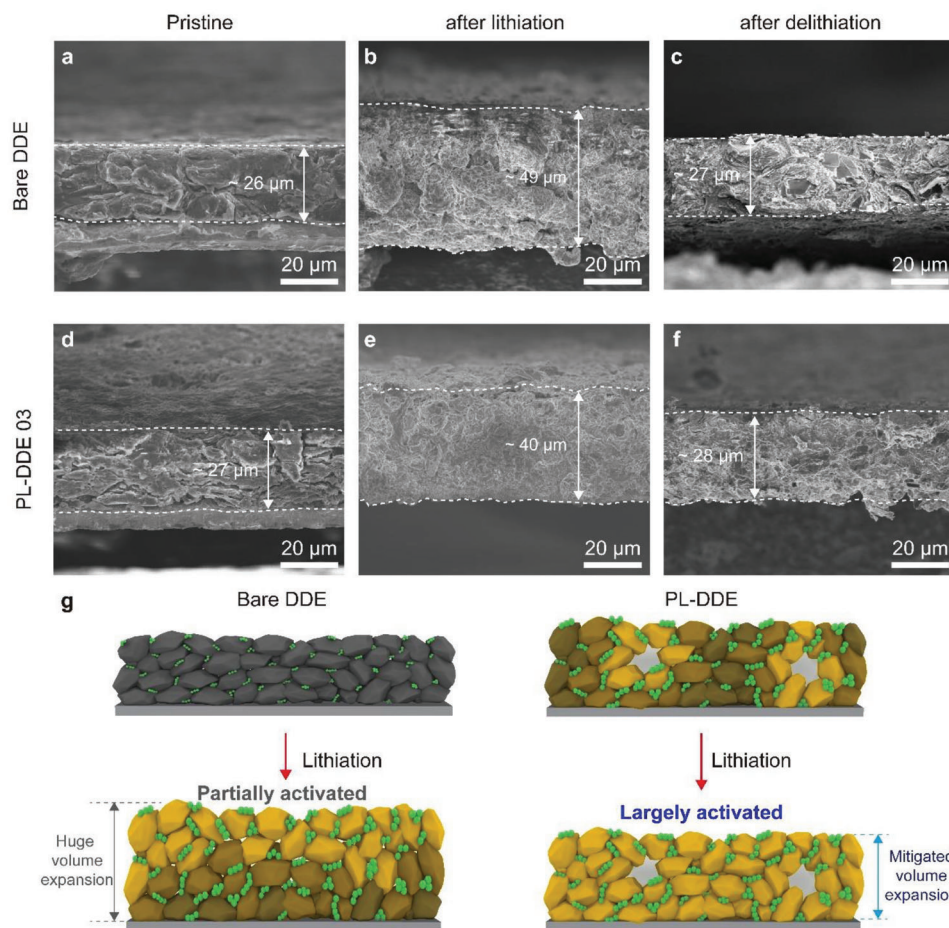


**Figure 5.** Cross-sectional SEM images of a–c) bare DDE and d–f) PL-DDE 03 after pressing, lithiation, and delithiation. g) Schematic illustration of lithiation behavior of the bare DDE and PL-DDE 03.

that pre-lithiation effects also emerge in the full cell system. The electrochemical impedance spectra of the cell with the DDEs after the first cycle are shown in Figure 6b. The cell with PL-DDE 03 demonstrated lower resistance than the cell with the bare DDE, especially in the mid- and low-frequency regions related to charge transport resistance ( $R_{ct}$ ). This result implies that the mitigated volume expansion by pre-lithiation effectively alleviates the deterioration of the electrode structure, allowing PL-DDE 03 to exhibit better charge transfer properties. The rate capability and capacity retention of full cells with DDEs were investigated in Figure 6c. PL-DDE 03 cells demonstrated 93.0, 83.9, 72.8, and 57.2% capacity retention at 0.2, 0.3, 0.5, and 1.0 C, respectively, which are slightly lower values than the cell with bare DDE (95.0, 86.9, 77.4, and 62.5% capacity retention at 0.2, 0.3, 0.5, and 1.0 C, respectively). However, in the 0.5/0.5 C charge/discharge cycling test, the bare DDE cell displayed a rapid capacity decrease and only showed capacity retention of 72.4% after 100 cycles. In contrast, the PL-DDE 03 cell showed stable capacity retention of 88.1% after 100 cycles. To reveal component changes of the DDEs after the cycling test, we performed an XPS analysis for the electrodes after the 100 cycles (0.5/0.5 C charge/discharge) (Figure S20, Supporting Information). In the C1s spectra after the cycling test, a clear  $\text{Li}_x\text{C}$  peak at 283 eV was observed in the bare DDE,<sup>[25]</sup>

while a significantly smaller  $\text{Li}_x\text{C}$  peak was observed in PL-DDE. Similarly,  $\text{Li}_x\text{Si}$  at around 96 eV was only observed in Si 2p spectrum of the bare DDE after cycles, but not of PL-DDE 03.<sup>[26]</sup> These XPS results indicate that PL-DDE 03 exhibits efficient lithiation/delithiation behavior even after long-term cycling, while the bare DDE showed an irreversible capacity loss during cycles. Therefore, the PL-DDE demonstrated excellent compatibility for applying practical use through LCO||Gr/Si full cell system test and showed continuously enhanced cycling performance.

### 3. Conclusion

In summary, we presented a new concept of a dry pre-lithiation method for DDEs using the direct transport of Li ions from the lithium metal powders to the active materials. Simultaneously added Li metal powder to the electrode contributes to enhancing the CEs by providing the Li source not only in the first cycle but also in prolonged cycling. In particular, the residual Li plays an important role in the activator to compensate for the active Li loss and promote the complete lithiation of all the active materials. In addition, facile interparticle diffusion of DDEs enables Li ions to easily spread throughout the entire active materials, which leads to uniform pre-lithiation of the electrode without local



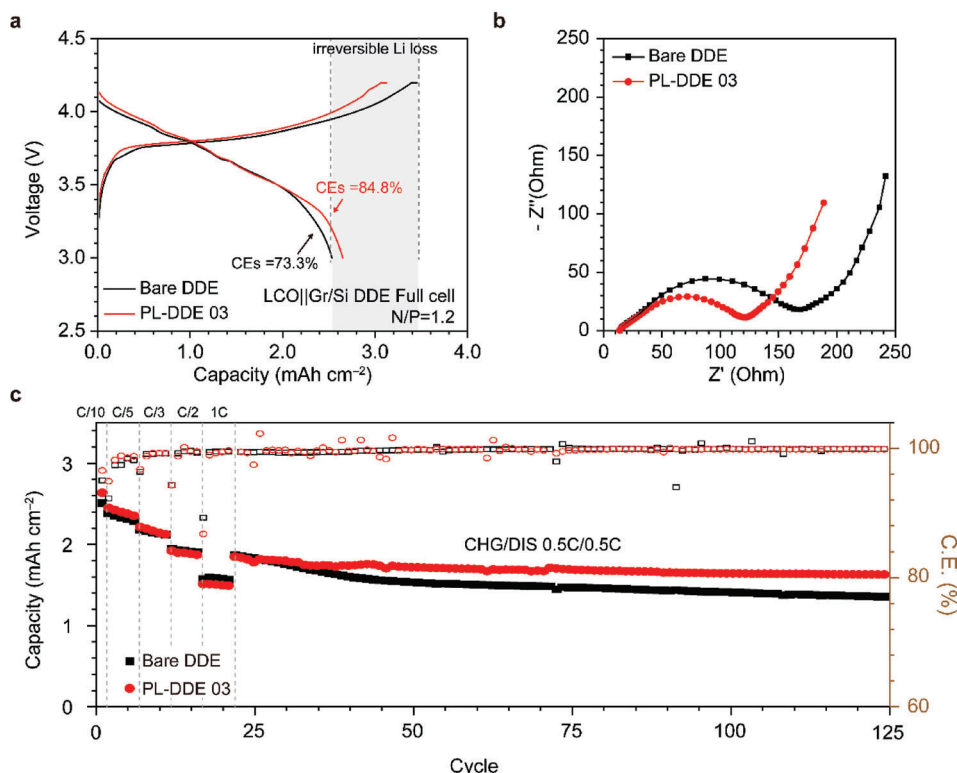


**Figure 6.** a) First charge-discharge voltage profiles of the full cells with bare DDE and PL-DDE 03. b) EIS results of the cells with the bare DDE and PL-DDE 03 after the initial charge-discharge cycle. c) Rate performance and cycle performance of the cell with bare DDE and PL-DDE 03.

overpotential of several active material particles. Owing to these merits, the PL-DDE realized a high areal and specific capacity of  $3.0 \text{ mAh cm}^{-2}$ , and  $602.1 \text{ mAh g}^{-1}$ , which is a comparable capacity with the theoretical capacity of the Gr/Si electrode ( $\sim 621 \text{ mAh g}^{-1}$ ). Uniform lithiation state and effective Li utilization of PL-DDE minimized volume expansion, resulting in superior cycle performance with stable CEs (85.2% retention with 99.6% CE at 200 cycles). Stable cycling of PL-DDE coupled with LCO cathode fully demonstrated its compatibility and superiority for ASSB application. These beneficial features of the PL-DDE will lead to a simple but effective design of DDE to achieve a more realistic high-energy density of ASSBs with stable cycle performance.

## Supporting Information

Supporting Information is available from the Wiley Online Library or from the author.

## Acknowledgements

J.L., D.J., and J.K. contributed equally to this work. This work was supported by the National Research Foundation of Korea (NRF) grant funded by the Korean government (MSIT) (No.NRF-2021M3H4A1A02048529) and the National Research Foundation of Korea (NRF-2022M3J1A1054326, NRF-2022M3J1A1085396) funded by the Ministry of Science and ICT.

## Conflict of Interest

The authors declare no conflict of interest.

## Data Availability Statement

The data that support the findings of this study are available from the corresponding author upon reasonable request.

## Keywords

all-solid-state batteries, diffusion-dependent electrodes, dry-state, graphite-silicon electrodes, pre-lithiation

Received: January 16, 2023  
Revised: April 11, 2023  
Published online: May 11, 2023

- [1] a) Z. Zhang, Y. Shao, B. Lotsch, Y.-S. Hu, H. Li, J. Janek, L. F. Nazar, C.-W. Nan, J. Maier, M. Armand, L. Chen, *Energy Environ. Sci.* **2018**, *11*, 1945; b) Y. Xiao, Y. Wang, S.-H. Bo, J. C. Kim, L. J. Miara, G. Ceder, *Nat. Rev. Mater.* **2020**, *5*, 105; c) Q. Zhao, S. Stalin, C.-Z. Zhao, L. A. Archer, *Nat. Rev. Mater.* **2020**, *5*, 229; d) T. Liu, Y. Yuan, X. Tao, Z. Lin, J. Lu, **2020**, *7*, 2001207; e) J. Janek, W. G. Zeier, *Nat. Energy* **2016**, *1*, 16141; f) A. Manthiram, X. Yu, S. Wang, *Nat. Rev. Mater.* **2017**, *2*, 16103; g) T. Ye, L. Li, Y. Zhang, *Adv. Funct. Mater.* **2020**, *30*, 2000077; h) T. Liu, Y. Yuan, X. Tao, Z. Lin, J. Lu, *Adv. Sci.* **2020**, *7*, 2001207.

- [2] a) H. Karami, M. F. Mousavi, M. Shamsipur, *J. Power Sources* **2003**, 124, 303; b) D. H. Shen, G. Halpert, *J. Power Sources* **1993**, 43, 327; c) K.-N. Jung, H.-S. Shin, M.-S. Park, J.-W. Lee, *ChemElectroChem* **2019**, 6, 3842.
- [3] a) T. Famprikis, P. Canepa, J. A. Dawson, M. S. Islam, C. Masquelier, *Nat. Mater.* **2019**, 18, 1278; b) J. C. Bachman, S. Muy, A. Grimaud, H.-H. Chang, N. Pour, S. F. Lux, O. Paschos, F. Maglia, S. Lupart, P. Lamp, L. Giordano, Y. Shao-Horn, *Chem. Rev.* **2016**, 116, 140; c) Y. Zhu, X. He, Y. Mo, *ACS Appl. Mater. Interfaces* **2015**, 7, 23685; d) J. Li, C. Ma, M. Chi, C. Liang, N. J. Dudney, *Adv. Energy Mater.* **2015**, 5, 1401408.
- [4] a) R. Koerver, I. Aygün, T. Leichtweiß, C. Dietrich, W. Zhang, J. O. Binder, P. Hartmann, W. G. Zeier, J. Janek, *Chem. Mater.* **2017**, 29, 5574; b) W. Zhang, D. A. Weber, H. Weigand, T. Arlt, I. Manke, D. Schröder, R. Koerver, T. Leichtweiss, P. Hartmann, W. G. Zeier, J. Janek, *ACS Appl. Mater. Interfaces* **2017**, 9, 17835; c) P. Knauth, *Solid State Ionics* **2009**, 180, 911; d) J. Park, K. T. Bae, D. Kim, W. Jeong, J. Nam, M. J. Lee, D. O. Shin, Y.-G. Lee, H. Lee, K. T. Lee, Y. M. Lee, *Nano Energy* **2021**, 79, 105456; e) J. Lee, S. Byun, H. Lee, Y. Roh, D. Jin, J. Lim, J. Song, C. B. Zdzakpasu, J. Park, Y. M. Lee, *Battery Energy* **2023**, 2, 20220061.
- [5] a) N. Kamaya, K. Homma, Y. Yamakawa, M. Hirayama, R. Kanno, M. Yonemura, T. Kamiyama, Y. Kato, S. Hama, K. Kawamoto, A. Mitsui, *Nat. Mater.* **2011**, 10, 682; b) Y. Kato, S. Hori, T. Saito, K. Suzuki, M. Hirayama, A. Mitsui, M. Yonemura, H. Iba, R. Kanno, *Nat. Energy* **2016**, 1, 16030; c) Y. J. Nam, D. Y. Oh, S. H. Jung, Y. S. Jung, *J. Power Sources* **2018**, 375, 93; d) D. H. Kim, D. Y. Oh, K. H. Park, Y. E. Choi, Y. J. Nam, H. A. Lee, S.-M. Lee, Y. S. Jung, *Nano Lett.* **2017**, 17, 3013; e) J. S. Kim, S. Jung, H. Kwak, Y. Han, S. Kim, J. Lim, Y. M. Lee, Y. S. Jung, *Energy Storage Mater.* **2023**, 55, 193; f) Y. S. Jung, D. Y. Oh, Y. J. Nam, K. H. Park, *Isr. J. Chem.* **2015**, 55, 472.
- [6] a) X. Chen, W. He, L.-X. Ding, S. Wang, H. Wang, *Energy Environ. Sci.* **2019**, 12, 938; b) A. Bielefeld, D. A. Weber, J. Janek, *J. Phys. Chem. C* **2019**, 123, 1626; c) F. Strauss, T. Bartsch, L. de Biasi, A. Y. Kim, J. Janek, P. Hartmann, T. Brezesinski, *ACS Energy Lett.* **2018**, 3, 992; d) G. T. Hitz, D. W. McOwen, L. Zhang, Z. Ma, Z. Fu, Y. Wen, Y. Gong, J. Dai, T. R. Hamann, L. Hu, E. D. Wachsman, *Mater. Today* **2019**, 22, 50; e) Y. He, S. Chen, L. Nie, Z. Sun, X. Wu, W. Liu, *Nano Lett.* **2020**, 20, 7136; f) T. Shi, Q. Tu, Y. Tian, Y. Xiao, L. J. Miara, O. Kononova, G. Ceder, *Adv. Energy Mater.* **2020**, 10, 1902881; g) J. Park, K. T. Kim, D. Y. Oh, D. Jin, D. Kim, Y. S. Jung, Y. M. Lee, *Adv. Energy Mater.* **2020**, 10, 2001563.
- [7] a) D. Cao, Y. Zhao, X. Sun, A. Natan, Y. Wang, P. Xiang, W. Wang, H. Zhu, *ACS Energy Lett.* **2020**, 5, 3468; b) D. Y. Oh, D. H. Kim, S. H. Jung, J.-G. Han, N.-S. Choi, Y. S. Jung, *J. Mater. Chem. A* **2017**, 5, 20771; c) D. H. Kim, Y.-H. Lee, Y. B. Song, H. Kwak, S.-Y. Lee, Y. S. Jung, *ACS Energy Lett.* **2020**, 5, 718; d) J. Zhang, H. Zhong, C. Zheng, Y. Xia, C. Liang, H. Huang, Y. Gan, X. Tao, W. Zhang, *J. Power Sources* **2018**, 391, 73; e) K. J. Kim, J. L. M. Rupp, *Energy Environ. Sci.* **2020**, 13, 4930; f) J.-M. Doux, Y. Yang, D. H. S. Tan, H. Nguyen, E. A. Wu, X. Wang, A. Banerjee, Y. S. Meng, *J. Mater. Chem. A* **2020**, 8, 5049; g) F. Han, J. Yue, C. Chen, N. Zhao, X. Fan, Z. Ma, T. Gao, F. Wang, X. Guo, C. Wang, *Joule* **2018**, 2, 497; h) S. Ohta, J. Seki, Y. Yagi, Y. Kihira, T. Tani, T. Asaoka, *J. Power Sources* **2014**, 265, 40; i) H. Nakamura, T. Kawaguchi, T. Masuyama, A. Sakuda, T. Saito, K. Kuratani, S. Ohsaki, S. Watano, *J. Power Sources* **2020**, 448, 227579.
- [8] a) J. Y. Kim, J. Park, M. J. Lee, S. H. Kang, D. O. Shin, J. Oh, J. Kim, K. M. Kim, Y.-G. Lee, Y. M. Lee, *ACS Energy Lett.* **2020**, 5, 2995; b) J. Y. Kim, J. Park, S. H. Kang, S. Jung, D. O. Shin, M. J. Lee, J. Oh, K. M. Kim, J. Zausch, Y.-G. Lee, Y. M. Lee, *Energy Storage Mater.* **2021**, 47, 289; c) J. Y. Kim, S. Jung, S. H. Kang, M. J. Lee, D. Jin, D. O. Shin, Y.-G. Lee, Y. M. Lee, *J. Power Sources* **2022**, 518, 230736; d) J. Y. Kim, S. Jung, S. H. Kang, J. Park, M. J. Lee, D. Jin, D. O. Shin, Y.-G. Lee, Y. M. Lee, *Adv. Energy Mater.* **2022**, 12, 2103108.
- [9] a) M. Li, J. Lu, Z. Chen, K. Amine, *Adv. Mater.* **2018**, 30, 1800561; b) D. Y. Oh, Y. J. Nam, K. H. Park, S. H. Jung, K. T. Kim, A. R. Ha, Y. S. Jung, *Adv. Energy Mater.* **2019**, 9, 1802927; c) K. Lee, S. Kim, J. Park, S. H. Park, A. Coskun, D. S. Jung, W. Cho, J. W. Choi, *J. Electrochem. Soc.* **2017**, 164, A2075; d) T. Ates, M. Keller, J. Kulisch, T. Adermann, S. Passerini, *Energy Storage Mater.* **2019**, 17, 204.
- [10] a) C. K. Chan, H. Peng, G. Liu, K. McIlwrath, X. F. Zhang, R. A. Huggins, Y. Cui, *Nat. Nanotechnol.* **2008**, 3, 31; b) P. G. Bruce, B. Scrosati, J.-M. Tarascon, *Angew. Chem., Int. Ed.* **2008**, 47, 2930; c) U. Kasavajjula, C. Wang, A. J. Appleby, *J. Power Sources* **2007**, 163, 1003; d) J. W. Choi, D. Aurbach, *Nat. Rev. Mater.* **2016**, 1, 16013; e) N. Liu, Z. Lu, J. Zhao, M. T. McDowell, H.-W. Lee, W. Zhao, Y. Cui, *Nat. Nanotechnol.* **2014**, 9, 187.
- [11] a) F. Wang, B. Wang, J. Li, B. Wang, Y. Zhou, D. Wang, H. Liu, S. Dou, *ACS Nano* **2021**, 15, 2197; b) J. Zhao, Z. Lu, H. Wang, W. Liu, H.-W. Lee, K. Yan, D. Zhuo, D. Lin, N. Liu, Y. Cui, *J. Am. Chem. Soc.* **2015**, 137, 8372; c) N. Liu, L. Hu, M. T. McDowell, A. Jackson, Y. Cui, *ACS Nano* **2011**, 5, 6487.
- [12] M. W. Forney, M. J. Ganter, J. W. Staub, R. D. Ridgley, B. J. Landi, *Nano Lett.* **2013**, 13, 4158.
- [13] K. H. Kim, J. Shon, H. Jeong, H. Park, S. J. Lim, J. S. Heo, *J. Power Sources* **2020**, 459, 228066.
- [14] a) Y. Zhu, W. Hu, J. Zhou, W. Cai, Y. Lu, J. Liang, X. Li, S. Zhu, Q. Fu, Y. Qian, *ACS Appl. Mater. Interfaces* **2019**, 11, 18305; b) Y. Sun, Y. Li, J. Sun, Y. Li, A. Pei, Y. Cui, *Energy Storage Mater.* **2017**, 6, 119; c) X. Zhang, H. Qu, W. Ji, D. Zheng, T. Ding, C. Abegglen, D. Qiu, D. Qu, *ACS Appl. Mater. Interfaces* **2020**, 12, 11589.
- [15] H. J. Kim, S. Choi, S. J. Lee, M. W. Seo, J. G. Lee, E. Deniz, Y. J. Lee, E. K. Kim, J. W. Choi, *Nano Lett.* **2016**, 16, 282.
- [16] K. Park, B.-C. Yu, J. B. Goodenough, *Adv. Energy Mater.* **2016**, 6, 1502534.
- [17] a) Z. Wang, Y. Fu, Z. Zhang, S. Yuan, K. Amine, V. Battaglia, G. Liu, *J. Power Sources* **2014**, 260, 57; b) H. Xu, S. Li, C. Zhang, X. Chen, W. Liu, Y. Zheng, Y. Xie, Y. Huang, J. Li, *Energy Environ. Sci.* **2019**, 12, 2991.
- [18] a) Y. Pang, X. Wang, X. Shi, F. Xu, L. Sun, J. Yang, S. Zheng, *Adv. Energy Mater.* **2020**, 10, 1902795; b) C. Wang, L. Zhang, H. Xie, G. Pastel, J. Dai, Y. Gong, B. Liu, E. D. Wachsman, L. Hu, *Nano Energy* **2018**, 50, 393.
- [19] a) D. Jin, J. Oh, A. Friesen, K. Kim, T. Jo, Y. M. Lee, M.-H. Ryou, *ACS Appl. Mater. Interfaces* **2018**, 10, 16521; b) D. Jin, J. Park, M.-H. Ryou, Y. M. Lee, *Adv. Mater. Interfaces* **2020**, 7, 1902113.
- [20] P. Bärmann, M. Mohrhardt, J. E. Frerichs, M. Helling, A. Kolesnikov, S. Klabunde, S. Nowak, M. R. Hansen, M. Winter, T. Placke, *Adv. Energy Mater.* **2021**, 11, 2100925.
- [21] a) S. Misra, N. Liu, J. Nelson, S. S. Hong, Y. Cui, M. F. Toney, *ACS Nano* **2012**, 6, 5465; b) A. Ulvestad, A. H. Reksten, H. F. Andersen, P. A. Carvalho, I. J. T. Jensen, M. U. Nagell, J. P. Mæhlen, M. Kirkengen, A. Y. Kozlov, *ChemElectroChem* **2020**, 7, 4349.
- [22] J. Park, S. S. Park, Y. S. Won, *Electrochim. Acta* **2013**, 107, 467.
- [23] a) T. D. Hatchard, J. R. Dahn, *J. Electrochem. Soc.* **2004**, 151, A838; b) Q. Shabir, A. Pokale, A. Loni, D. R. Johnson, L. T. Canham, R. Fenolosa, M. Tymczenko, I. Rodríguez, F. Meseguer, A. Cros, A. Cantarero, *Silicon* **2011**, 3, 173.
- [24] T. Krauskopf, B. Mogwitz, C. Rosenbach, W. G. Zeier, J. Janek, *Adv. Energy Mater.* **2019**, 9, 1902568.
- [25] a) G. G. Eshetu, T. Diemant, S. Grueone, R. J. Behm, S. Laruelle, M. Armand, S. Passerini, *ACS Appl. Mater. Interfaces* **2016**, 8, 16087; b) K. Kanamura, S. Shiraishi, H. Tamura, Z. i. Takehara, *J. Electrochem. Soc.* **1994**, 141, 2379; c) S. Link, M. Kurniawan, A. Dimitrova, S. Krischok, A. Bund, S. Ivanov, *Electrochim. Acta* **2021**, 380, 138216; d) S. Malmgren, K. Ciosek, R. Lindblad, S. Plogmaker, J. Kühn, H. Rensmo, K. Edström, M. Hahlin, *Electrochim. Acta* **2013**, 105, 83.

- [26] a) E. Radvanyi, E. De Vito, W. Porcher, S. Jouanneau Si Larbi, *J. Anal. At. Spectrom.* **2014**, 29, 1120; b) B. Philippe, R. Dedryvère, J. Allouche, F. Lindgren, M. Gorgoi, H. Rensmo, D. Gonbeau, K. Edström, *Chem. Mater.* **2012**, 24, 1107; c) B. Philippe, R. Dedryvère, M. Gorgoi, H. Rensmo, D. Gonbeau, K. Edström, *J. Am. Chem. Soc.* **2013**, 135, 9829; d) R. Endo, T. Ohnishi, K. Takada, T. Masuda, *J. Phys. Chem.* **2020**, 11, 6649.
- [27] a) Z. Liu, A. Borodin, G. Li, X. Liu, Y. Li, F. Endres, *J. Phys. Chem. C* **2020**, 124, 300; b) S.-K. Otto, L. M. Riegger, T. Fuchs, S. Kayser, P. Schweitzer, S. Burkhardt, A. Henss, J. Janek, *Adv. Mater. Interfaces* **2022**, 9, 2102387; c) G. F. Dewald, S. Ohno, M. A. Kraft, R. Koerver, P. Till, N. M. Vargas-Barbosa, J. Janek, W. G. Zeier, *Chem. Mater.* **2019**, 31, 8328; d) L. Ye, X. Li, *Nature* **2021**, 593, 218.
- [28] Y. Jeon, H. K. Noh, H.-K. Song, *Sci. Rep.* **2017**, 7, 14879.